AGU PUBLICATIONS

JGR

Journal of Geophysical Research: Space Physics

RESEARCH ARTICLE
10.1002/2015JA021932

Key Points:
- Unusually large equatorial zonal electric field at dusk sector due to eastward PPEF
- Enhanced electric field limited to a narrow longitudinal sector centered on sunset terminator
- Unique electrodynamic conditions at sunset terminator are responsible for large zonal electric field

Correspondence to:
S. Tulasi Ram,
tulasi@iigs.iigm.res.in

Citation:
Tulasi Ram, S., et al. (2016), Duskside enhancement of equatorial zonal electric field response to convection electric fields during the St. Patrick's Day storm on 17 March 2015, *J. Geophys. Res. Space Physics*, *121*, 538–548, doi:10.1002/2015JA021932.

Received 18 SEP 2015
Accepted 6 DEC 2015
Accepted article online 10 DEC 2015
Published online 11 JAN 2016

Duskside enhancement of equatorial zonal electric field response to convection electric fields during the St. Patrick's Day storm on 17 March 2015

S. Tulasi Ram[1], T. Yokoyama[2], Y. Otsuka[3], K. Shiokawa[3], S. Sripathi[1], B. Veenadhari[1], R. Heelis[4], K. K. Ajith[1], V. S. Gowtam[1], S. Gurubaran[1], P. Supnithi[5], and M. Le Huy[6]

[1]Indian Institute of Geomagnetism, Navi Mumbai, India, [2]National Institute for Information and Communications Technology, Tokyo, Japan, [3]Institute for Space-Earth Environmental Research, Nagoya University, Nagoya, Japan, [4]W. B. Hanson Center for Space Sciences, University of Texas at Dallas, Richardson, Texas, USA, [5]Faculty of Engineering, King Mongkut's Institute of Technology Ladkrabang, Bangkok, Thailand, [6]Institute of Geophysics, Vietnamese Academy of Science and Technology, Hanoi, Vietnam

Abstract The equatorial zonal electric field responses to prompt penetration of eastward convection electric fields (PPEF) were compared at closely spaced longitudinal intervals at dusk to premidnight sectors during the intense geomagnetic storm of 17 March 2015. At dusk sector (Indian longitudes), a rapid uplift of equatorial *F* layer to >550 km and development of intense equatorial plasma bubbles (EPBs) were observed. These EPBs were found to extend up to 27.13°N and 25.98°S magnetic dip latitudes indicating their altitude development to ~1670 km at apex. In contrast, at few degrees east in the premidnight sector (Thailand-Indonesian longitudes), no significant height rise and/or EPB activity has been observed. The eastward electric field perturbations due to PPEF are greatly dominated at dusk sector despite the existence of background westward ionospheric disturbance dynamo (IDD) fields, whereas they were mostly counter balanced by the IDD fields in the premidnight sector. In situ observations from SWARM-A and SWARM-C and Communication/Navigation Outage Forecasting System satellites detected a large plasma density depletion near Indian equatorial region due to large electrodynamic uplift of *F* layer to higher than satellite altitudes. Further, this large uplift is found to confine to a narrow longitudinal sector centered on sunset terminator. This study brings out the significantly enhanced equatorial zonal electric field in response to PPEF that is uniquely confined to dusk sector. The responsible mechanisms are discussed in terms of unique electrodynamic conditions prevailing at dusk sector in the presence of convection electric fields associated with the onset of a substorm under southward interplanetary magnetic field B_z.

1. Introduction

The high latitude-low latitude coupled neutral and electrodynamic processes during active geomagnetic periods cause substantial modifications in the equatorial and low-latitude ionosphere-thermosphere system. Particularly, the global scale equatorial zonal electric field, which is usually eastward (westward) during daytime (nighttime), undergo several changes during the storm periods and can significantly alter the equatorial electrodynamical processes. In general, these zonal electric field perturbations are mainly due to two important processes, known as prompt penetration electric fields (PPEF) and ionospheric disturbance dynamo (IDD). The dynamic reconnection between solar wind and Earth's magnetosphere causes the development of high-latitude electric fields through field-aligned currents which can penetrate promptly to equatorial latitudes through Earth-ionosphere wave guide [*Nishida*, 1968; *Kikuchi et al*., 2000]. On the other hand, the disturbance dynamo electric fields are induced via global scale thermospheric wind circulation due to Joule heating at high latitudes [*Blanc and Richmond*, 1980]. The PPEF can occur almost simultaneously with the sudden changes in the *z* component of interplanetary magnetic field (IMF B_z) and induces short-lived (~30 min to 2 h) perturbations in the equatorial zonal electric fields [*Senior and Blanc*, 1984; *Kelley et al*., 2003]. Whereas, the disturbance dynamo fields can be observed with a few hours delay and are usually long lasting for several hours via thermospheric wind dynamo action.

During southward IMF B_z periods, the region 1 (R1) field aligned currents (FAC) are often stronger than the region 2 (R2) currents (undershielding), and the enhanced convection electric field causes eastward (westward) PPEFs in dayside (nightside) ionosphere [*Nishida*, 1968; *Kikuchi et al*., 1996; *Kikuchi et al*., 2000] which are in the same direction to the quiet time global scale dawn-dusk zonal electric field at the equator. On the other hand,

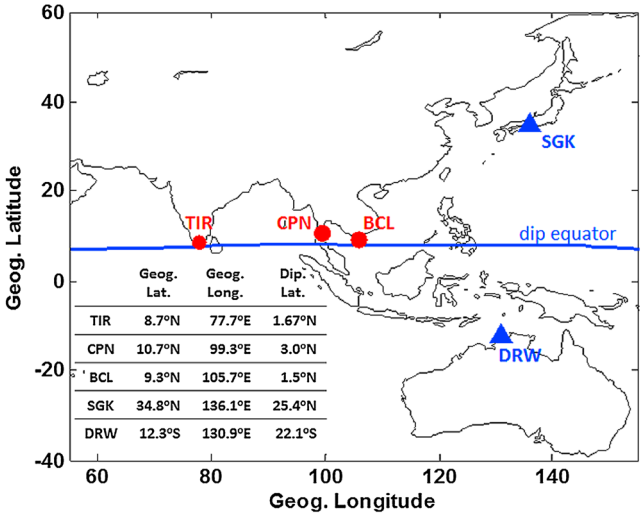

Figure 1. Geographic locations of ionosondes and Fabry-Perot interferometers used in this study. The geographic coordinates and dip latitudes are indicated in the figure.

the sudden northward turning of IMF B_z makes the R2 currents to be momentarily stronger than R1-FAC (overshielding) and causes electric field perturbations that are opposite polarity to the quiet time zonal electric field [*Rastogi and Patel*, 1975; *Kelley et al*., 1979, 2003]. These PPEFs associated with sudden southward (northward) turning of IMF B_z are generally referred as convection (overshielding) electric fields. The eastward convection electric fields in dayside can significantly redistribute the *F* region plasma through reinforced equatorial ionization anomaly (EIA) and cause positive ionospheric storms at low-midlatitude regions [*Mannucci et al*., 2005; *Tulasi Ram et al*., 2008; *Veenadhari et al*. 2010; *Balan et al*., 2012]. Further, the eastward PPEFs can enhance the development of equatorial plasma bubbles (EPBs) at postsunset sectors and can cause severe disruption of transionospheric radio communication links, hence, very important in view of space based communication and navigational applications [*Basu et al*., 2001; *Martinis et al*., 2005; *Basu et al*., 2005]. It is also shown that long-duration eastward PPEF can occur under steady southward IMF B_z condition for several hours [*Huang et al*., 2005; *Huang et al*., 2007] that can cause the development of EPBs continuously over a very wide postsunset longitudinal sector [*Tulasi Ram et al*., 2008; *Tulasi Ram et al*., 2015].

Numerical model simulations show that the polarity of convection electric fields is usually eastward at dusk sector and can extend up to premidnight hours of ~22–23 LT [*Nopper and Carovillano*, 1978; *Tsunomura and Araki*, 1984; *Senior and Blanc*, 1984]. Though the observations are sparse, limited studies reported the effects of the eastward convective PPEF during the premidnight hours. For example, *Abdu et al*. [1998] have shown the penetration of DP 2 electric field fluctuations to equatorial ionosphere at dusk sector with enhanced amplitudes of eastward convection electric fields toward nightside. Using the in situ vertical plasma drifts from Republic of China Satellite-1 during 1999 to 2004, *Fejer et al*. [2008] have shown that the convective PPEFs are eastward in the postsunset sector and turns to westward around 23 LT. Recently, *Chakrabarty et al*. [2015] have reported the eastward PPEF effects during 2100–2200 LT that strengthened the spread *F* in equatorial ionosphere. Hence, it is important to investigate the effects of PPEFs from dusk to premidnight sector, simultaneously, at closely spaced longitudinal intervals in order to understand the relative amplitudes of zonal electric field perturbations and its influence on the development of EPBs. Therefore, in this paper, a case study on the response of equatorial ionosphere to convective PPEFs is investigated simultaneously at closely spaced longitudinal intervals from dusk to premidnight sector using both ground-based and satellite in situ observations during an intense geomagnetic storm occurred on 17 March 2015 and the relative amplitudes of eastward electric field perturbations are studied in the context of development of EPBs. Further, the possible influence of substorm expansion onset on penetration of eastward convection electric fields and the effects of coexistent disturbance dynamo electric fields at different local time sectors were discussed.

2. Observations

The response of equatorial and low-latitude ionosphere during the intense geomagnetic storm of 17 March 2015 has been closely investigated from dusk to premidnight sectors using a chain of ionosondes in Southeast Asian longitudes that span across the Indian-Thailand-Vietnam regions. For example, Figure 1 shows the locations of three ionosondes considered in this study. The ionosonde at Indian equatorial station, Tirunelveli (TIR), is of Canadian Advanced Digital Ionosonde (CADI) model operated by Indian Institute of Geomagnetism, India. The other two ionosondes at Chumphon (CPN), Thailand, and Bac Lieu (BCL),

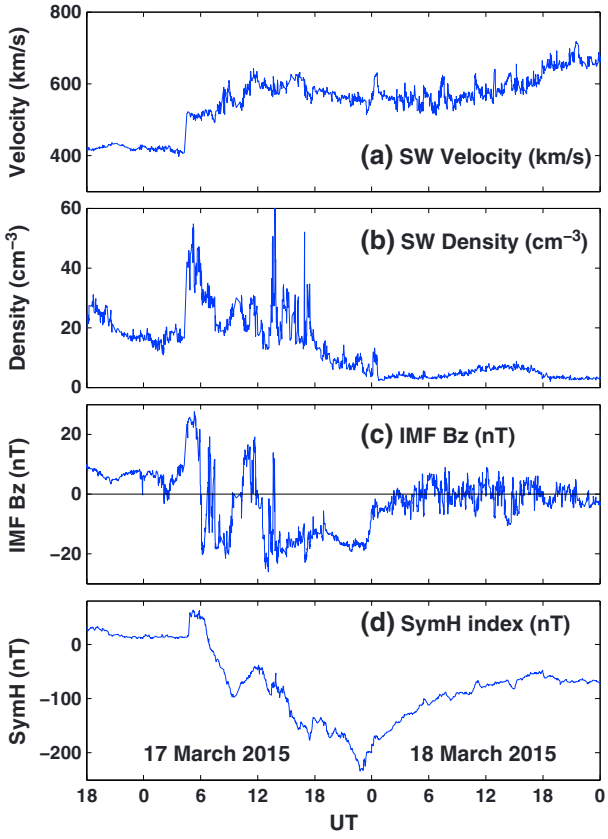

Figure 2. Temporal variations of (a) solar wind velocity, (b) solar wind density, (c) *z* component of interplanetary magnetic field (IMF B_z), and (d) *SYM-H* index.

Vietnam, were frequency modulated continuous wave ionosondes operated under SouthEast Asia Low-latitude Ionospheric Network (SEALION) by National institute of Information and Communications Technology, Japan (http://seg-web.nict.go.jp/sealion/). The geographic coordinates and dip latitudes of the ionosonde locations were shown in Figure 1. As can be observed from Figure 1, the three ionosondes at TIR, CPN, and BCL were located along the dip equator at closely spaced longitudinal intervals, hence, considered to investigate the equatorial zonal electric field perturbations due to PPEFs at different local times from dusk to premidnight sectors. All the ionosonde observations considered in this study were obtained at 10 min intervals. Further, the observations from two Fabry-Perot interferometers that are simultaneously operated at Shigaraki (SGK), Japan [*Shiokawa et al.*, 2003], and Darwin (DRW), Australia [*Shiokawa et al.*, 2012], were considered to examine the thermospheric neutral wind variations associated with ionospheric disturbance dynamo during this storm period. The SGK and DRW are located in northern and southern midlatitudes, respectively, at nearly conjugate locations. In addition to above mentioned ground based observations, the satellite in situ ion density measurements from C/NOFS (Communication/Navigation Outage Forecasting System) and SWARM-A, SWARM-B, and SWARM-C (European Space Agency Magnetic Field Mission) were also considered to examine the local time variations in the zonal electric field perturbations and the presence of EPBs. The 1 min data of *SYM-H*, *AU*, and *AL* indices were taken from Space Physics Data Facility (SPDF) at http://omniweb.gsfc.nasa.gov/ow_min.html. The 1 min data of interplanetary solar wind parameters observed from Wind satellite at L1-orbit and time shifted to bow shock nose were obtained from SPDF (http://omniweb.gsfc.nasa.gov/form/sc_merge_min1.html). The 5 min averages of energetic electron fluxes from GOES 15 satellite at geosynchronous orbit were taken from Coordinated Data Analysis Web (CDAWeb) at http://cdaweb.gsfc.nasa.gov/istp_public/. The horizontal component of geomagnetic field observations from ground based magnetometers at four stations, namely, Ascension Island (ASC, 7.95°S, 15°W, 24°S dip latitude), Mbour (MBO, 14.38°N, 16.97°W, 3.53°N dip latitude), Guam (GUA, 13.59°N, 144.87°E, 6.23°N dip latitude), and Kakioka (KAK, 36.23°N, 140.18°E, 30.8°N dip latitude) from INTERMAGNET (http://www.intermagnet.org/) were considered in this study.

3. Results

The magnetic filament eruption from sunspot AR2297 on the Sun at the early hours of 15 March has launched a Coronal Mass Ejection (CME) which has hit the Earth's magnetosphere around 0430 UT on 17 March 2015. Figure 2 shows the variations of solar wind parameters observed from WIND along with symmetrical ring current index, *SYM-H*. Both the solar wind velocity and density (Figures 2a and 2b) exhibits sudden enhancement from its steady state values at ~0430 UT indicating the arrival of CME shock. The impingement of CME shock on Earth's magnetosphere resulted in a sudden storm commencement with *SYM-H* raised to 67 nT by ~0448 UT. The *z* component of interplanetary magnetic field (IMF B_z) (Figure 2c) which is northward at initial phase, turned

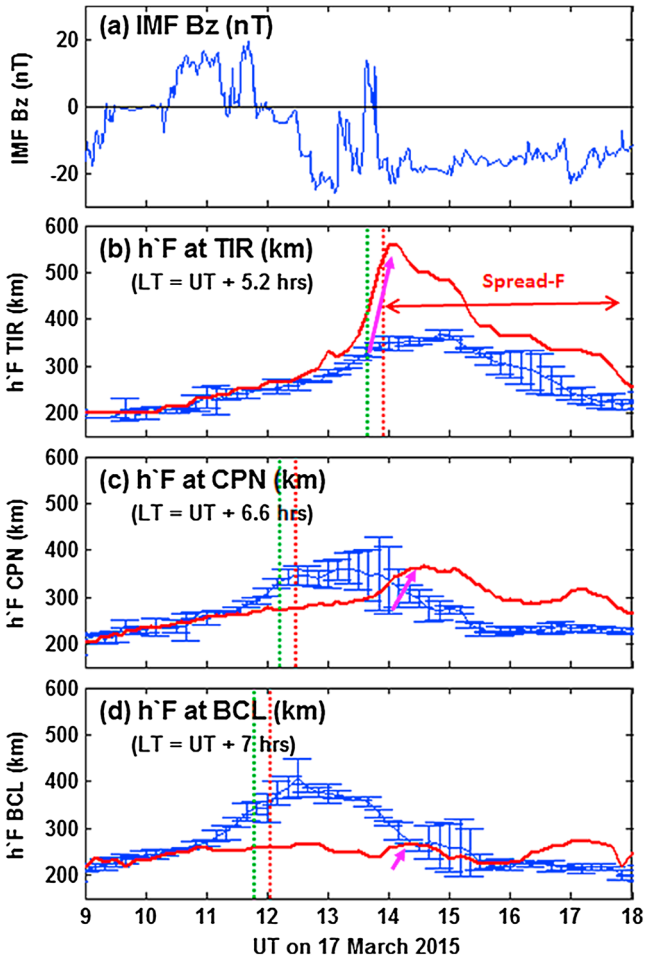

Figure 3. Temporal variations of (a) IMF B_z and the virtual base *F* layer height (h'F) at (b) Tirunelveli (TIR), (c) Chumphon (CPN), and (d) Bac Lieu (BCL) during 9–18 UT of 17 March 2015. The solid red curves in Figures 3b–3d represent the h'F variations on 17 March, and the blue curves with error bars indicate the previous 3 day mean h'F variations. The green and red vertical dotted lines represent the times of *E* region and *F* region sunset terminators, respectively. The pink arrows indicate the increase of h'F at the three stations with substantially enhanced amplitude at dusk sector (TIR) compared to premidnight (CPN and BCL) sector.

to southward at 0600 UT causing the magnetic reconnection and the main phase onset of a geomagnetic storm. After a few initial fluctuations, the IMF B_z remained southward till 0930 UT and the ring current enhancement caused *SYM-H* index to reach approximately −100 nT (Figure 2d). The northward reversal of IMF B_z between 0930 and 1200 UT caused a brief recovery of *SYM-H* index to −38 nT. However, the IMF B_z again turned to southward at ~1230 UT and more or less remained steady southward for more than 11 h. This long-duration continuous southward IMF B_z facilitated continuous magnetic reconnection and enhanced ring current with *SYM-H* reaching a peak negative excursion of −232 nT at 2304 UT, becoming the strongest geomagnetic storm in the solar cycle 24 till date. *Singh et al.* [2015] have investigated the low-latitude ionospheric response exclusively over Indian sector during the different phases of this storm. However, in this study, we mainly focus our investigation on steady southward IMF B_z phase after 1230 UT and compare the equatorial zonal electric response over Indian and southeast Asian longitudinal which are in dusk to premidnight sectors.

Figure 3a shows the close view of *z* component of interplanetary magnetic field (IMF B_z) variation from 0900 to 1800 UT of 17 March 2015. It can be observed from this figure that the IMF B_z is mostly northward between 1000 and 1200 UT and turns to southward around ~1230 UT. Since then, the IMF B_z is steadily southward except for two short period northward deflections at ~1310 and 1330 UT. Figures 3b–3d show the *F* layer base (virtual) height (h'F) variations at equatorial stations of TIR, CPN, and BCL that are longitudinally separated at close intervals. The red thick curves in Figures 3b–3d represent the h'F variation on the storm day (17 March) as a function of universal time and the blue curves with error bars indicate the previously quiet 3 day mean h'F variation at the respective stations. The green and red dotted vertical lines in each panel represent the times of *E* region (110 km) and *F* region (200 km) sunsets, respectively. It can be observed from Figure 3b that the h'F over TIR is similar to its quiet day mean values up to 1200, started to increase from 1230 UT and dramatically elevated to greater than ~550 km by 1400 UT which is substantially larger than its quiet day mean postsunset enhancement. Large upward surge of equatorial *F* layer is observed around 1330–1350 UT near sunset terminator where the h'F increased rapidly from 366 km to 510 km. It should be noted here that this large upward drift exactly coincides with the time of usual postsunset height rise (PSSR) at TIR due to prereversal enhancement of electric field (PRE) around local sunset [*Singh et al.*, 2015]. However, the h'F excursion to above 550 km on 17 March is substantially larger compared to its quiet day PSSR as can be seen from Figure 3b. This indicates that the additional zonal electric field probably associated with the penetration of eastward convection electric fields contributed for this

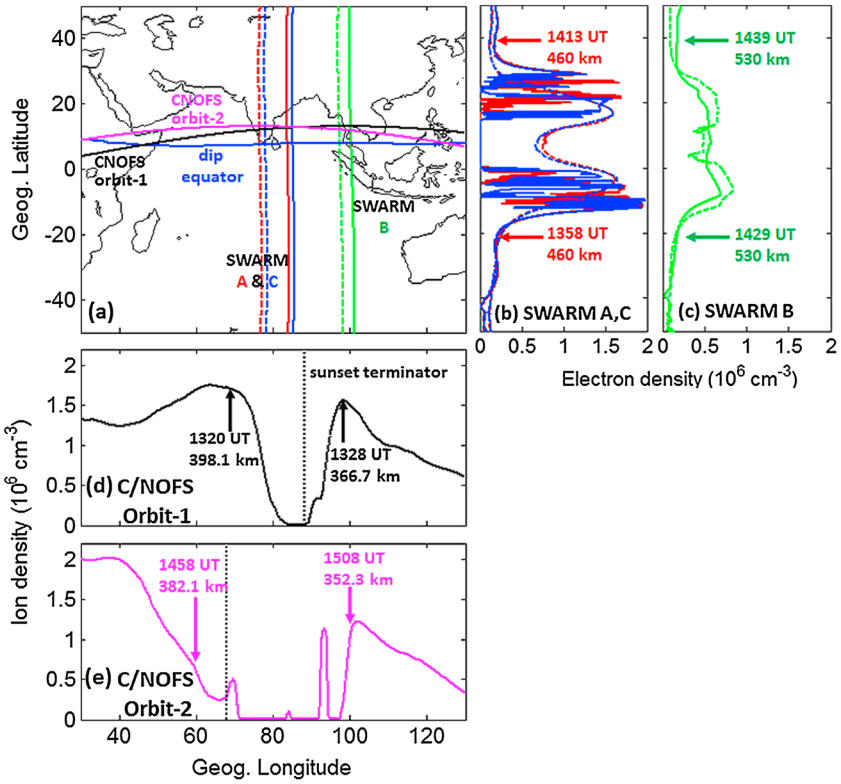

Figure 4. In situ ion density observations from a nearly simultaneous orbits of SWARM-A, SWARM-B, and SWARM-C and C/NOFS during ~1320–1500 UT of 17 March 2015 over Indian (dusk) and Thailand (premidnight) longitudinal sectors. (a) The ground tracks of SWARM and C/NOFS satellites along with the location of dip equator. The dotted lines indicate the SWARM orbits on the previous day around the same time. (b and c) The latitudinal variation of in situ electron density observations along the orbits from SWARM-A and SWARM-C, and SWARM-B. (d and e) The longitudinal variations of in situ ion density from C/NOFS during two successive orbits. The exact timings and their orbital altitudes are indicated in Figures 4b–4d. The vertical black dotted lines in Figures 4d and 4e represent the locations of sunset terminator corresponding to C/NOFS altitudes (refer to text for more details).

unusually large vertical uplift of equatorial *F* layer at the dusk sector. The range spread *F* echoes began to appear from 1350 UT, become intense at 1400 UT and continued to occur throughout that night. The h'F values from 1400 UT are scaled from bottommost trace of range spread *F* echoes, and their accuracy is subject to some degree of uncertainty due to the presence of spread *F*. From Figure 3c, it can be observed that the PSSR at Chumphon (CPN) is suppressed on storm day than its quiet day mean values. This is probably due to prevailing westward electric field perturbations associated with disturbance dynamo (discussed later in section 4). However, it is interesting to note that the h'F at CPN also exhibits an increase from 290 to 360 km during 1330–1430 UT, but this increase at CPN is very small compared to at TIR. No significant spread *F* is observed at CPN except faint echoes between 1420 and 1610 UT. Similarly at BCL (Figure 3d), the postsunset height rise significantly suppressed; however, a slight increase in h'F can be seen during 1340–1430 UT as indicated by pink arrows. Therefore, the h'F observations from Figure 3 clearly indicate the prompt penetration of eastward convection electric fields to equatorial latitudes around ~1330 to 1430 UT at dusk to premidnight sector. However, the amplitude of response, in terms of upward drift of equatorial *F* layer, is substantially larger at dusk sector and decreases as moving into the premidnight sector.

With a view to further examine the variability of equatorial zonal electric field and the development of EPBs over dusk to premidnight sector in response to the observed eastward PPEF, the in situ ion density measurements from C/NOFS and SWARM (A, B, and C) satellites were examined. While C/NOFS is a low-inclination (13°) satellite in elliptical orbit [*de La Beaujardière and the C/NOFS Definition Team*, 2004], the SWARM-A, SWARM-B, and SWARM-C are polar satellites in circular orbits with ~88° inclination [*Olsen et al.*, 2013]. Figure 4a shows the ground tracks of nearly simultaneous C/NOFS and SWARM-A, SWARM-B, and SWARM-C

satellite passes over Indian-Southeast Asian longitudes (dusk to premidnight sector) around the same period when the PPEF effects observed from ground-based ionosondes at TIR, CPN, and BCL. The solid curves in red, green, and blue indicate the SWARM-A, SWARM-B, and SWARM-C tracks on 17 March, respectively, and the dotted lines indicate the same for previous day. The ground tracks of two successive C/NOFS orbits are shown as black and pink curves in low-inclination orbits. The blue line indicates the location of dip equator. Figures 4b and 4c show the in situ electron density variations from planar Langmuir probe on board the SWARM along their orbits using the same color code assigned for their orbit tracks. It can be observed from Figure 4a that the SWARM-A and SWARM-C are orbiting in dusk sector over Indian longitudes (~85°E) around 1400 UT and the SWARM-B passes in premidnight sector over Indonesia-Thailand longitudes (~100°E) around 30 min later (~1430 UT). The exact timings of satellite passes and their orbital altitudes are shown in Figures 4b and 4c. It is interesting to observe from Figure 4b that the ion density values measured on SWARM-A and SWARM-C show less than 1000 particles per cm^3 over the dip equatorial latitudes which is unusually smaller than its quiet time values (dotted lines). This unusually low ion density values ($<1000\,cm^{-3}$) over equatorial region observed by SWARM-A and SWARM-C can be attributed to the uplift of *F* layer to higher than SWARM altitude due to eastward PPEF. The increase of h'F to greater than ~550 km at TIR at 1400 UT (Figure 3b) which is higher than the SWARM orbital altitude of 460 km further supports this argument. Further, the ion density exhibits large fluctuations which are the clear signatures of intense EPB irregularities up to 29.75°N and 13.22°S geographic (27.13°N and 25.98°S magnetic dip) latitudes. This indicates that EPBs over this region have risen to an apex altitude of ~1670 km over the equator according to field aligned nature of plasma bubble irregularities. Hence, the results from both ground based ionosonde and SWARM-A and SWARM-C in situ observations, consistently, indicate the substantially enhanced eastward zonal electric field that caused large uplift of equatorial *F* layer to >550 km and development of EPBs which further altitudinally grown to an apex altitude of ~1670 km over Indian (dusk sector) equatorial region.

Interestingly, about 15° toward east in the premidnight sector, the SWARM-B does not observe any effects of eastward PPEF and/or signatures of EPBs (Figure 4c). Further, compared to its previous quiet day observations (dotted curves) around the same longitudinal sector, the measured ion density values on 17 March are smaller, and the equatorial ionization anomaly (EIA) structure appears to be suppressed. This is consistent with the smaller increase in h'F over CPN and BCL (Figures 3c and 3d) indicating that the effects of eastward PPEF is weak in this premidnight sector, hence, could not be observed by SWARM-B at 530 km altitude. Further, the weak eastward PPEF effects did not cause any EPB activity at this premidnight sector.

The most interesting observation comes from the in situ ion density measurements from CINDI (Coupled Ion Neutral Dynamics Investigation) on board the low-inclination satellite C/NOFS orbiting at ~400–350 km altitudes (Figures 4d and 4e). The black vertical dotted lines in Figures 4d and 4e represent the locations of sunset terminator at C/NOFS altitude. It can be observed from Figure 4d that the C/NOFS orbit around 1320 UT detects large ion density depletion over Indian region at a narrow band of longitude sector centered on the local sunset terminator. This large ion density depletion observed at local sunset terminator indicates the elevation of *F* layer to much higher altitudes and the C/NOFS is slicing through the bottommost region of *F* layer, hence, detecting very low ion density values. This is consistent with the large upward surge of equatorial h'F observed at TIR due to eastward PPEF. Interestingly, this enhanced upward drift of *F* layer is mostly limited to a narrow band of longitudes (±10°) centered on sunset terminator indicating the unique feature of enhanced equatorial zonal electric field that confined to dusk sector. The C/NOFS's revisit over the same region after ~97 min also detected the large ion density depletion over Indian sector (Figure 4e). However, the density depleted region is observed to be expanded westward causing large ion density depletion over a wider longitudinal sector. The westward expansion of depleted region can be attributed to westward movement of sunset terminator in the presence of eastward PPEFs causing large uplift of *F* layer to above the C/NOFS altitude. The salient feature that should be noted from the C/NOFS observations is that the enhanced zonal electric field and the large uplift of *F* layer is mostly centered on sunset terminator and that moves westward along with the sunset terminator. On the other hand, at a few degrees east in the premidnight sector, the zonal electric field perturbation is very small as can be observed as a sharp eastward boundary of ion density depleted region from C/NOFS (Figure 4d) and suppressed EIA feature from SWARM-B (Figure 4c) at ~100°E longitude. These results were further consistent with the ground based ionosonde observations at CPN and BCL in the premidnight sector.

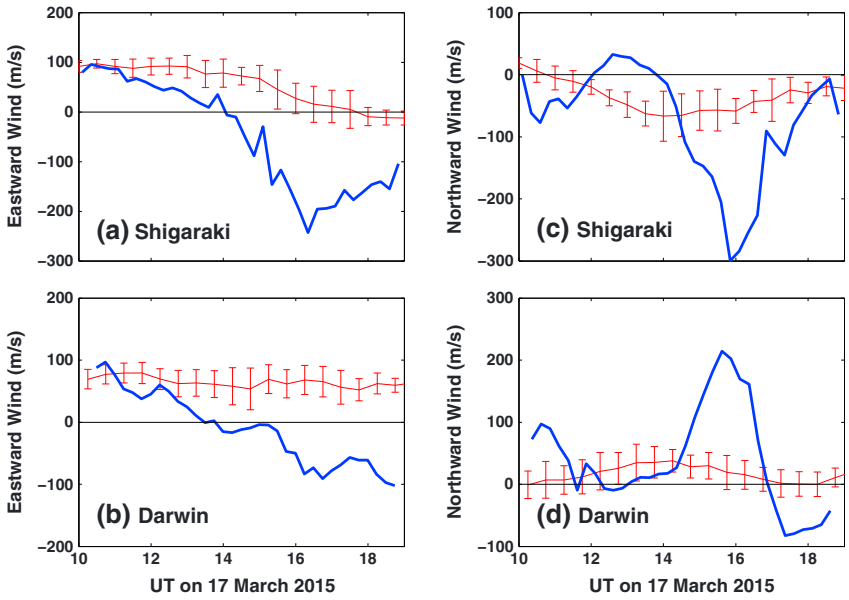

Figure 5. Thermospheric zonal (positive east) and meridional (positive northward) wind observations at 630 nm emission lines from Fabry-Perot interferometers at Shigaraki (SGK) and Darwin (DRW) during 10–19 UT of 17 March 2015. The red curves with error bars represent the quiet time mean zonal wind variations during the vernal equinox months of March–April at the respective stations.

4. Discussion

The zonal electric field perturbations in the equatorial ionosphere during geomagnetic storm periods are generally interpreted in terms of PPEFs and ionospheric disturbance dynamo fields. While the transient PPEFs appear at equatorial latitudes almost simultaneously with the sudden changes in the interplanetary electric field (IEFy) [*Nishida*, 1968; *Kikuchi et al*., 1996], the disturbance dynamo electric field effects appear with a delay of ~3–4 h [*Fejer and Scherliess*, 1997; *Fejer*, 2002; *Fujiwara et al*., 1996; *Xiong et al*., 2015]. On many occasions, the both PPEF and disturbance dynamo fields are coexist, and the net effect at equatorial ionosphere is determined by their relative amplitudes and polarities. Considering the solar wind energy input and onset of geomagnetic storm as early at ~0600 UT, it is expected that the ionospheric disturbance dynamo process may have already been active by that time of observed PPEF effects shown in Figures 3 and 4. The suppressed postsunset height rise at CPN and BCL (Figures 3c and 3d) further indicates presence of westward electric field perturbations. With a view to further examine the disturbance neutral wind variations during this period, the thermospheric neutral winds measured by two Fabry-Perot interferometers at nearly conjugate locations of Shigaraki (SGK) and Darwin (DRW) were considered. Figure 5 shows the thermospheric zonal (a and b, positive eastward) and meridional wind (c and d, positive northward) variations derived from 630 nm airglow emission line during 1000 to 1900 UT at SGK (a and c) and DRW (b and d). The quiet time mean zonal and meridional wind variations for the vernal equinox months of March and April during 2012–2015 at the respective stations were also shown in red curves with error bars for comparison. It can be observed that the zonal winds at both SGK and DRW (Figures 5a and 5b) were initially eastward with velocity of ~100 m/s around 1000 UT which is similar to its quite time mean values. However, the eastward wind at both SGK and DRW decreased rapidly with time and becomes westward at 1400 UT. The zonal wind becomes largely westward with approximately −240 m/s at SGK and −91 m/s at DRW by ~1620 UT indicating the large neutral wind disturbance. The meridional winds at both SGK and DRW (Figures 5c and 5d) also significantly deviated from its quiet time mean variations indicating the neutral wind disturbance throughout the night. The meridional wind at SGK turns southward (equatorward) around 1400 UT and exhibits a large equatorward wind surge of ~ −300 m/s at 1550 UT. The meridional wind at DRW also exhibits large equatorward wind with a maximum of ~210 m/s around 1535 UT. The large westward zonal wind and equatorward meridional wind observed at both SGK and DRW that significantly deviate from their quiet time mean variations indicates the large-scale thermospheric wind disturbance associated with ionospheric

disturbance dynamo [*Blanc and Richmond*, 1980]. Although the zonal wind at SGK and DRW turned westward around 1400 UT, the decrease in eastward wind to below its quiet time standard deviation can be observed starting from 1200 UT. This indicates that the disturbance dynamo winds were already setup from 1200 UT. The disturbance wind driven dynamo fields induce westward zonal electric field perturbations at equatorial and low latitudes in the day to premidnight local time sector [*Blanc and Richmond*, 1980]. Further, the suppressed postsunset height rise at CPN and BCL during 1100–1400 UT indicates the presence of westward zonal electric field perturbations which could be attributed to ionospheric disturbance dynamo. These preexisted westward disturbance dynamo electric fields may probably counter balance the eastward PPEF associated with southward turning of IMF B_z at 1230 UT, and the net eastward electric field perturbation effect become small at CPN and BCL in the premidnight sector as seen in Figures 3 and 4.

However, at TIR, the ascent of equatorial *F* layer starting from 1230 UT with southward turning of IMF B_z and a large upward surge around 1330–1350 UT (Figure 3b) indicates the dominant role of eastward PPEF effects in the dusk sector. On the other hand, no significant uplift of *F* layer is observed during this period at CPN and BCL which were located at premidnight sector (Figures 3c and 3d). This result clearly suggests that the equatorial zonal electric field response to penetration of eastward convection electric field is significantly enhanced at dusk sector (TIR) than at premidnight sector (CPN and BCL). *Maruyama et al*. [2005] have compared the storm time electric field perturbations due to PPEF and IDD and mentioned that the penetration electric fields are dominant during the daytime while the magnitudes of disturbance dynamo and penetration electric fields are nearly comparable during nighttimes. *Abdu et al*. [1998] and *Sanders et al*. [2012] have reported that the evening equatorial ionosphere responds more aggressively to PPEFs which are consistent with the results observed in this study.

At first, this enhanced eastward electric field response at TIR (dusk sector) can be explained as due to eastward PPEF which adds positively to the regular prereversal enhancement of zonal electric field at local sunset and the combined effects would be responsible for the large uplift of equatorial *F* layer at dusk as interpreted by *Singh et al*. [2015]. However, one can observe from Figure 3b that the quiet time postsunset rise (PSSR) of h′F is only from ~284 to 347 km during 1300–1400 UT (blue curve with error bars). Also, the IMF B_z is not steadily southward during this period and exhibits northward fluctuations at ~1309 and 1330 UT. Thus, the large increase in h′F observed over TIR cannot be fully explained by the regular PSSR added with eastward PPEF as the IMF B_z is fluctuating northward during this period. This suggests that some other process may simultaneously be operational to augment the additional eastward electric field to support the uplift of equatorial *F* layer to greater than 550 km at dusk sector.

Another important factor to be considered is the role of substorms. Several earlier studies have reported the penetration of high-latitude electric fields to low-latitude ionosphere during substorms [*Gonzales et al*., 1979; *Kikuchi et al*., 2003; *Sastri et al*., 2003; *Huang*, 2009, 2012, and references therein]. However, the penetration electric fields during the substorms found to exhibit a complex variability. For example, *Gonzales et al*. [1979], *Kikuchi et al*. [2000, 2003], and *Sastri et al*. [2001, 2003] have shown that the low-latitude ionospheric electric field disturbance is westward and the geomagnetic field disturbance is negative (negative bay) in the dayside during onset of a substorm expansion. However, *Huang et al*. [2004] and *Huang* [2009, 2012] have demonstrated that during the geomagnetic storm time substorms under southward IMF B_z periods, the dayside low-latitude ionospheric electric field disturbance at substorm onset is eastward and the geomagnetic field disturbance is positive (positive bay). Hence, the possible effects of substorms on the large uplift of equatorial *F* layer observed over TIR were examined during the present storm period. For example, Figures 6a–6c show the variations of IMF B_z, *AU*, and *AL* indices and the energetic electron fluxes measured at geosynchronous orbit by GOES 15 (135°W) satellite. It can be observed from the Figure 6b that the *AL* index exhibits a rapid decrease around 1325 UT indicating the onset of a substorm expansion. This is preceded by the sudden increase in the electron fluxes measured by GOES 15 at geosynchronous orbit (Figure 6c) in postmidnight sector indicating the injection of energetic particles from the tail to inner magnetosphere, the so-called sawtooth event [*Huang et al*., 2003]. It can be noticed from Figure 6a that the IMF B_z is southward at the onset of substorm. Figure 6d shows the variations in horizontal component of geomagnetic field at two stations ASC and MBO which were in the noon sector (LT $\approx$ UT $-$ 1 h) at the time of substorm onset. These two stations were selected from the noon sector such that one station (MBO) is at geomagnetically low latitude (3.53°N dip latitude) and other (ASC) is close to midlatitudes (24°S dip latitude). Similarly, Figure 6e shows the *H* component variations at low-latitude to midlatitude

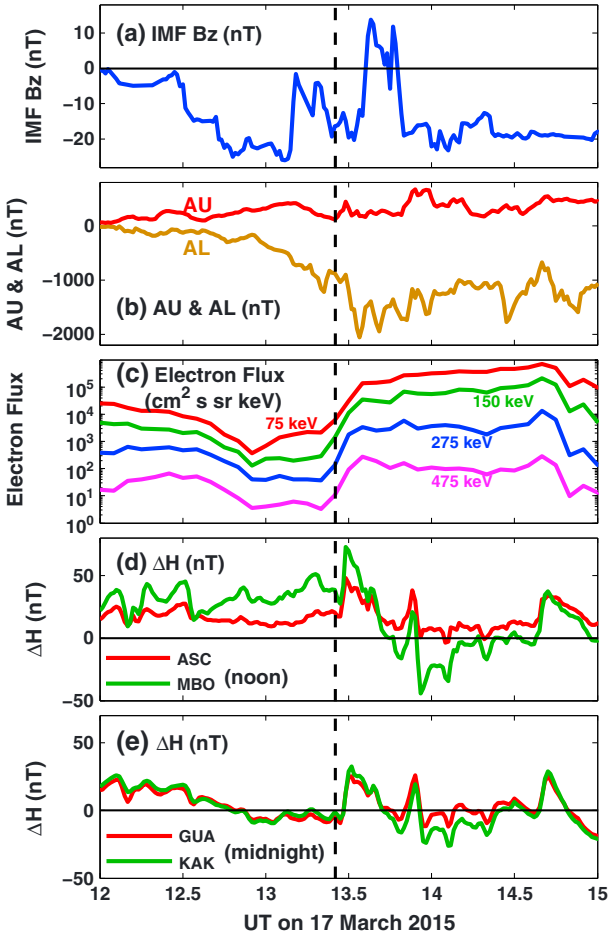

Figure 6. The temporal variations of (a) IMF B_z, (b) *AU* and *AL* indices, (c) energetic electron fluxes from GOES 15 at geosynchronous orbit, (d) Δ*H* at ASC and MBO from the noon sector, and (e) Δ*H* variations at GUA and KAK from the midnight sector during 1200 to 1500 UT on 17 March 2015. The black dotted vertical line indicates the time of substorm onset.

stations GUA (6.3°N dip latitude) and KAK (30.8°N dip latitude) from the midnight sector (LT ≈ UT + 9.5 h). Since the enhanced ring current during the main phase of storm causes a large decrease in *H* component of geomagnetic field, a 4 h running mean is subtracted from the *H* values to reduce the ring current effects similar to that adopted in *Huang* [2009, 2012] and the residual (Δ*H*) variations are presented in Figures 6d and 6e. The conspicuous feature is the simultaneous increase in Δ*H* indicating a geomagnetic positive bay at both dayside (noon sector) and nightside (midnight sector) low-latitude to midlatitude stations. These observations are similar to those reported by *Huang* [2009, 2012] and indicate the enhanced eastward electric field perturbation and geomagnetic positive bay in dayside associated with the onset of substorm.

Huang [2009, 2012] have suggested that the increased convection at substorm onset causes an enhanced magnetospheric electric field which promptly penetrates to dayside low-latitude ionosphere. This induced eastward electric field perturbation due to substorm causes an increase in *H* component of geomagnetic field (positive bay) through eastward Pedersen current. The Pedersen current is significantly enhanced at equatorial latitudes due to Cowling effect [*Haerendal and Eccles*, 1992] in dayside ionosphere. However, the Pedersen conductivity exhibits a large gradient across the sunset terminator due to large *E* region conductivity on dayside and negligible conductivity on nightside. Thus, the enhanced Pedersen current by convection electric field is subjected to large conductivity gradient across sunset terminator and the positive charges will be accumulated at the terminator. The associated divergent electric field at terminator is eastward and maps along the equipotential field lines to *F* region. This additional electric field strengthens the upward drift of equatorial *F* layer in addition to the primary PPEF as observed at TIR in the dusk sector. Thus, the net combined eastward electric field effects dominated over the preexisted disturbance dynamo electric fields and caused large upward surge of equatorial *F* layer and development of EPBs over dusk sector as observed from C/NOFS and SWARM-A and SWARM-C. Further, this additional electric field appears to be limited to a narrow longitudinal sector centered on sunset terminator due to large conductivity gradient as observed from C/NOFS and SWARM-A and SWARM-C in situ observations (Figures 4d and 4e). *Abdu et al*. [1998] have reported similar enhanced vertical drift due to penetration of DP2 fluctuations near sunset which is attributed to the unique electrodynamic conditions at the sunset terminator. However, this phenomenon is not effective in the premidnight sector due to negligible *E* region Pedersen conductivity during nighttimes. Therefore, the equatorial zonal electric field perturbations to PEEFs were small in the premidnight sector as observed from SWARM-B (Figure 4c) and ground-based ionosonde observations at CPN and BCL at ~100°E longitude sector.

5. Conclusions

Using a longitudinal chain of ionosondes along with nearly simultaneous passes of SWARM-A, SWARM-B, and SWARM-C and C/NOFS satellites, the equatorial zonal electric field responses to eastward convection electric fields were compared at a closely spaced intervals from dusk to premidnight sectors. At the dusk (Indian) sector, the enhanced eastward electric field caused a large upward surge of equatorial *F* layer to >550 km (h'F at TIR) and subsequent development of spread *F* (Figure 3b). The significantly elevated equatorial *F* layer facilitated the EPBs to grow up to an apex altitude of ~1670 km and found to extend up to 27.13°N and 25.98°S magnetic dip latitudes (Figure 4b). In contrast, at a few degrees east in the premidnight sector, no significant height raise and/or ESF activity has been observed as evidenced from Ionosondes at CPN, BCL (Figures 3c and 3d), and from SWARM-B (Figure 4c). The distinctly different responses observed between SWARM-A and SWARM-C, and SWARM-B over Indian and Indonesian sectors which are separated by only ~15° (1 h in LT) brings out the unique feature of remarkably enhanced duskside zonal electric field in comparison with premidnight sector, despite the presence of background westward disturbance dynamo fields. Further, the C/NOFS in situ observations (Figure 4d) provide additional evidence that the significantly large electrodynamic uplift of equatorial *F* layer is confined only to a narrow longitudinal sector centered on sunset terminator. The uniquely enhanced duskside equatorial zonal electric field response is deeply investigated and the responsible mechanisms were discussed in terms of large gradient in *E* region conductivity across the sunset terminator at low latitudes and the presence of enhanced eastward Pedersen current driven by convection electric fields associated with the onset of a substorm under southward IMF B_z conditions. This study is first of this kind that compares the equatorial electric field response to PPEFs at closely spaced longitudinal intervals from dusk to premidnight sectors and provides important insights on the unique storm time electrodynamic conditions prevailing at dusk sector with adequate observational evidence using both ground based and space borne observations.

Acknowledgments

This work is supported by STEL, Nagoya University under the international joint research program 2015 and partially supported by DST, Government of India through project GITA/DST/TWN/P-47/2013. The measurement at Darwin has been carried out in collaboration with the IPS Radio and Space Services, Bureau of Meteorology, Australia. The work of K. Shiokawa is supported by JSPS Core-to-Core Program, B. Asia-Africa Science Platforms, JSPS KAKENHI (grants 20244080, 5247080, and 15H05815) and the IUGONET Project from MEXT, Japan. The ionosonde data of CPN and BCL are available through SEALION network (http://seg-web.nict.go.jp/sealion/). Sripathi is the PI of CADI ionosonde data at TIR and can be contacted for any data request at sripathi@iigs.iigm.res.in. The authors acknowledge the open data policy of SWARM (https://earth.esa.int/web/guest/missions/esa-operational-eo-missions/swarm) and C/NOFS-CINDI (http://cindispace.utdallas.edu/). The solar wind parameters from Wind satellite, *SYM-H*, *AU*, and *AL* indices were obtained from SPDF, NASA, USA (http://omniweb.gsfc.nasa.gov/ow_min.html), and the energetic electron fluxes data from GOES 15 at geosynchronous orbit were obtained from CDAWeb (http://cdaweb.gsfc.nasa.gov/istp_public/). The magnetometer data from ASC, MBO, GUA, and KAK were taken from Intermagnet (http://www.intermagnet.org/index-eng.php).

References

Abdu, M. A., J. H. Sastri, H. Luhr, H. Tachihara, T. Kitamura, N. B. Trivedi, and J. H. A. Sobral (1998), DP 2 electric field fluctuations in the dusk-time dip equatorial ionosphere, *Geophys. Res. Lett.*, *25*(9), 1511–1514.

Balan, N., J. Y. Liu, Y. Otsuka, S. Tulasi Ram, and H. Lühr (2012), Ionospheric and thermospheric storms at equatorial latitudes observed by CHAMP, ROCSAT, and DMSP, *J. Geophys. Res.*, *117*, A01313, doi:10.1029/2011JA016903.

Basu, S., S. Basu, K. M. Groves, H. C. Yeh, S. Y. Su, F. J. Rich, P. J. Sultan, and M. J. Keskinen (2001), Response of the equatorial ionosphere in the South Atlantic region to the great magnetic storm of July 15, 2000, *Geophys. Res. Lett.*, *28*, 3577–3580.

Basu, S., S. Basu, K. M. Groves, E. MacKenzie, M. J. Keskinen, and F. J. Rich (2005), Near-simultaneous plasma structuring in the midlatitude and equatorial ionosphere during magnetic superstorms, *Geophys. Res. Lett.*, *32*, L12S05, doi:10.1029/2004GL021678.

Blanc, M., and A. D. Richmond (1980), The ionospheric disturbance dynamo, *J. Geophys. Res.*, *85*, 1669–1688.

Chakrabarty, D., D. Rout, R. Sekar, R. Narayanan, G. D. Reeves, T. K. Pant, B. Veenadhari, and K. Shiokawa (2015), Three different types of electric field disturbances affecting equatorial ionosphere during a long-duration prompt penetration event, *J. Geophys. Res. Space Physics*, *120*, 4993–5008, doi:10.1002/2014JA020759.

de La Beaujardière, O., and The C/NOFS Definition Team (2004), C/NOFS: A mission to forecast scintillations, *J. Atmos. Sol. Terr. Phys.*, *66*, 1573, doi:10.1016/j.jastp.2004.07.030.

Fejer, B. G. (2002), Low latitude storm time ionospheric electrodynamics, *J. Atmos. Sol. Terr. Phys.*, *64*, 1401.

Fejer, B. G., and L. Scherliess (1997), Emperical models of storm time equatorial zonal electric fields, *J. Geophys. Res.*, *102*, 24,047–24,056.

Fejer, B. G., J. W. Jensen, and S.-Y. Su (2008), Seasonal and longitudinal dependence of equatorial disturbance vertical plasma drifts, *Geophys. Res. Lett.*, *35*, L20106, doi:10.1029/2008GL035584.

Fujiwara, H., S. Maeda, H. Fukunishi, T. Fuller-Rowell, and D. S. Evans (1996), Global variations of thermospheric winds and temperatures caused by substorm energy injection, *J. Geophys. Res.*, *101*(A1), 225–239, doi:10.1029/95JA01157.

Gonzales, C. A., M. C. Kelley, B. G. Fejer, J. F. Vickrey, and R. F. Woodman (1979), Equatorial electric fields during magnetically disturbed conditions: 2. Implications of simultaneous auroral and equatorial measurements, *J. Geophys. Res.*, *84*(A10), 5803–5812, doi:10.1029/JA084iA10p05803.

Haerendal, G., and J. V. Eccles (1992), The role of the equatorial electrojet in the evening ionosphere, *J. Geophys. Res.*, *97*, 1181–1192.

Huang, C. S., J. C. Foster, and M. C. Kelley (2005), Long-duration penetration of the planetary electric field to the low-altitude ionosphere during the main phase of magnetic storms, *J. Geophys. Res.*, *110*, A11309, doi:10.1029/2005JA011202.

Huang, C. S., S. Sazykin, J. L. Chau, N. Maruyama, and M. C. Kelley (2007), Penetration electric fields: Efficiency and characteristic time scale, *J. Atmos. Sol. Terr. Phys.*, *69*, 1135–1146.

Huang, C.-S. (2009), Eastward electric field enhancement and geomagnetic positive bay in the dayside low-latitude ionosphere caused by magnetospheric substorms during sawtooth events, *Geophys. Res. Lett.*, *36*, L18102, doi:10.1029/2009GL040287.

Huang, C.-S. (2012), Statistical analysis of dayside equatorial ionospheric electric fields and electrojet currents produced by magnetospheric substorms during sawtooth events, *J. Geophys. Res.*, *117*, A02316, doi:10.1029/2011JA017398.

Huang, C.-S., J. C. Foster, G. D. Reeves, G. Le, H. U. Frey, C. J. Pollock, and J.-M. Jahn (2003), Periodic magnetospheric substorms: Multiple space-based and ground-based instrumental observations, *J. Geophys. Res.*, *108*(A11), 1411, doi:10.1029/2003JA009992.

Huang, C.-S., J. C. Foster, L. P. Goncharenko, G. D. Reeves, J. L. Chau, K. Yumoto, and K. Kitamura (2004), Variations of low-latitude geomagnetic fields and *Dst* index caused by magnetospheric substorms, *J. Geophys. Res.*, *109*, A05219, doi:10.1029/2003JA010334.

Kelley, M. C., B. Fejer, and C. Gonzales (1979), An explanation for anomalous equatorial ionospheric electric fields associated with a northward turning of the interplanetary magnetic field, *Geophys. Res. Lett.*, *6*, 301–304.
Kelley, M. C., J. J. Makela, J. L. Chau, and M. J. Nicolls (2003), Penetration of the solar wind electric field into the magnetosphere/ionosphere system, *Geophys. Res. Lett.*, *30*(4), 1158, doi:10.1029/2002GL016321.
Kikuchi, T., H. Luhr, T. Kitamura, O. Saka, and K. Schlegel (1996), Direct penetration of the polar electric fields to the equator during a DP 2 event as detected by the auroral and equatorial magnetometer chains and the EISCAT radar, *J. Geophys. Res.*, *101*, 17,161–17,173.
Kikuchi, T., H. Luhr, K. Schlegel, H. Tachihara, M. Shinohara, and T. L. Kitamura (2000), Penetration of auroral electric fields to the equator during a substorm, *J. Geophys. Res.*, *105*, 23,251–23,252.
Kikuchi, T., K. K. Hashimoto, T.-I. Kitamura, H. Tachihara, and B. Fejer (2003), Equatorial counterelectrojets during substorms, *J. Geophys. Res.*, *108*(A11), 1406, doi:10.1029/2003JA009915.
Mannucci, A. J., B. T. Tsurutani, B. A. Iijima, A. Komjathy, A. Saito, W. D. Gonzalez, F. L. Guarnieri, J. U. Kozyra, and R. Skoug (2005), Dayside global ionospheric response to the major interplanetary events of October 29–30, 2003 "Halloween Storms", *Geophys. Res. Lett.*, *32*, L12S02, doi:10.1029/2004GL021467.
Martinis, C. R., M. J. Mendillo, and J. Aarons (2005), Toward a synthesis of equatorial spread *F* onset and suppression during geomagnetic storms, *J. Geophys. Res.*, *110*, A07306, doi:10.1029/2003JA010362.
Maruyama, N., A. D. Richmond, T. J. Fuller-Rowell, M. V. Codrescu, S. Sazykin, F. R. Toffoletto, R. W. Spiro, and G. H. Millward (2005), Interaction between direct penetration and disturbance dynamo electric fields in the storm-time equatorial ionosphere, *Geophys. Res. Lett.*, *32*, L17105, doi:10.1029/2005GL023763.
Nishida, A. (1968), Coherence of geomagnetic DP 2 fluctuations with interplanetary magnetic variations, *J. Geophys. Res.*, *73*, 5549–5559, doi:10.1029/JA073i017p05549.
Nopper, R. W., and R. L. Carovillano (1978), Polar-equatorial coupling during magnetically active periods, *Geophys. Res. Lett.*, *5*(8), 699–702, doi:10.1029/GL005i008p00699.
Olsen, N., et al. (2013), The swarm satellite constellation application and research facility (SCARF) and SWARM data products, *Earth Planet. Space*, *65*, 1189–1200.
Rastogi, R. G., and V. L. Patel (1975), Effect of interplanetary magnetic field on ionosphere over the magnetic equator Proc, *Indian Acad. Sci.*, *82A*, 121–141.
Sanders, T., C. Huang, and D. M. Ober (2012), Local time variations of penetration electric fields during intense magnetic storms, AGU. Fall meeting, 2012AGUFMSA42A08S.
Sastri, J. H., Y. Kamide, and K. Yumoto (2003), Signatures for magnetospheric substorms in the geomagnetic field of dayside equatorial region: Origin of the ionospheric component, *J. Geophys. Res.*, *108*(A10), 1375, doi:10.1029/2003JA009962.
Sastri, J., J. Rao, D. Rao, and B. Pathan (2001), Daytime equatorial geomagnetic H field response to the growth phase and expansion phase onset of isolated substorms: Case studies and their implications, *J. Geophys. Res.*, *106*, 29,925–29,933, doi:10.1029/2001JA900120.
Senior, C., and M. Blanc (1984), On the control of magnetospheric convection by the spatial distribution of ionospheric conductivities, *J. Geophys. Res.*, *89*, 261–284.
Shiokawa, K., T. Kadota, Y. Otsuka, T. Ogawa, T. Nakamura, and S. Fukao (2003), A two-channel Fabry-Perot interferometer with thermoelectric-cooled CCD detectors for neutral wind measurement in the upper atmosphere, *Earth Planets Space*, *55*, 271–275.
Shiokawa, K., Y. Otsuka, S. Oyama, S. Nozawa, M. Satoh, Y. Katoh, Y. Hamaguchi, Y. Yamamoto, and J. Meriwether (2012), Development of low-cost sky-scanning Fabry-Perot interferometers for airglow and auroral studies, *Earth Planets Space*, *64*, 1033–1046.
Singh, R., S. Sripathi, S. Sreekumar, S. Banola, K. Emperumal, P. Tiwari, and S. Kumar (2015), Low latitude ionosphere response to super geomagnetic storm of 17/18 March 2015: Results from a chain of ground based observations over Indian sector, *J. Geophys. Res. Space Physics*, *120*, doi:10.1002/2015JA021509.
Tsunomura, S., and T. Araki (1984), Numerical analysis of equatorial enhancement of geomagnetic sudden commencement, *Planet. Space Sci.*, *32*(5), 599–604, doi:10.1016/0032-0633(84)90109-0.
Tulasi Ram, S., P. V. S. Rama Rao, D. S. V. V. D. Prasad, K. Niranjan, S. Gopi Krishna, R. Sridharan, and S. Ravindran (2008), Local time dependent response of post sunset ESF during geomagnetic storms, *J. Geophys. Res.*, *113*, A07310, doi:10.1029/2007JA012922.
Tulasi Ram, S., K. Sandeep, S.-Y. Su, B. Veenadhari, and S. Ravindran (2015), The influence of Corotating Interaction Region (CIR) driven geomagnetic storms on the development of equatorial plasma bubbles (EPBs) over wide range of longitudes, *Adv. Space Res.*, *55*, 535–544.
Veenadhari, B., S. Alex, T. Kikuchi, A. Shinbori, R. Singh, and E. Chandrasekhar (2010), Penetration of magnetospheric electric fields to the equator and their effects on low latitude ionosphere during intense geomagnetic storms, *J. Geophys. Res.*, *115*, A03305, doi:10.1029/2009JA014562.
Xiong, C., H. Luhr, and B. G. Fejer (2015), Global features of the disturbance winds during storm time deduced from CHAMP observations, *J. Geophys. Res. Space Physics*, *120*, 5137–5150, doi:10.1002/2015JA021302.